Multiload procedure to measure the acoustic scattering matrix of a duct discontinuity for higher order mode propagation conditions

Azzedine Sitel, Jean-Michel Ville,[a] and Felix Foucart
Laboratoire Roberval FRE UTC-CNRS No. 2833, Université de Technologie de Compiègne, BP 20529 F60205, Compiègne Cedex, France

(Received 2 February 2006; revised 8 August 2006; accepted 18 August 2006)

A procedure for measuring the acoustic scattering matrix coefficients of a duct discontinuity for higher order acoustic duct mode propagation conditions is described and tested. The technique requires measurement of pressure waves per mode coming in and out of the discontinuity. Assuming N cut-on modes, the $(2N)^2$ scattering matrix coefficients are determined after repeating the experiment for N linearly independent pressure distributions for at least two load configurations. Experiments were conducted for a straight duct and a reactive chamber. A good agreement was found between experiment and theory except near cut-off frequencies. The overdetermination method based on four loads was shown to improve the results. An analytical simulation of the experiment was developed to compute the influence on the $[S]$ calculation of an error in temperature and total modal pressure assumed to be representative of a real measurement situation. This simulation with a discussion explains the discrepancies between experiment and theory. The test with the chamber shows that the load method fails as expected in determining the coefficients associated to the wave coming in the discontinuity from the open end side because of the property of the middle duct to filter modes making the results very sensitive to uncertainties. © *2006 Acoustical Society of America.* [DOI: 10.1121/1.2354040]

PACS number(s): 43.20.Ye, 43.20.Mv [LLT] Pages: 2478–2490

I. INTRODUCTION

Sound propagation in duct systems is a problem of considerable practical interest for automotive, building, and aeronautic industries. A pipe system is usually considered as a network of straight ducts coupled together via various passive elements such as mufflers, bends, T-sections, etc. In order to analyze and optimize sound transmission, reflection, and radiation through and from those basic elements a formalism based on transfer matrix method[1,2] has been developed and most often used by manufacturers to design, for example, exhaust lines and air conditioning circuits. The scattering matrix formalism which uses the traveling wave amplitudes as state variables has been shown to be more attractive than transfer or mobility matrices since it reflects the fundamental waveguide nature of the problem allowing one to develop, for example, a general proposal for analyzing acoustic two-port networks[3,4] or to deduce acoustic energy dissipation or production in a multiport.[5]

Over the years a number of papers have been published on techniques based on two-loads and two source methods to perform measurements of the scattering matrix for plane wave propagation condition.[6,7]

Until now no specific measurement procedure which can be applied in higher order mode propagation conditions has been achieved. Only investigations on experimental methods to measure reflection and transmission matrices of discontinuities in a duct have been conducted.[8,9]

The aim of the paper is to present and test a method to measure the scattering matrix $[S]$ of a discontinuity for higher order mode propagation conditions. Unlike the reflection or transmission matrices, the scattering matrix of size $2N \times 2N$ (N being the number of cut-on modes) gives a more complete description of the discontinuity. Indeed it is independent of the open end duct conditions and can then be integrated in computer programs used for the conception of complex duct networks.

In Sec. II, after presenting the definition of the scattering matrix, the theory which the method is based on is described. In Sec. III, the experimental facility, the two duct discontinuities tested, and the procedure which leads to the determination of the scattering matrix are detailed. In the Sec. IV the experimental results are compared with theory for both duct configurations. Moreover an analytical simulation of the experiment is performed to study the sensibility of the $[S]$ coefficients to some parameters of the experiment such as temperature, microphone locations, and modal coefficients and used to explain some discrepancies observed between experiment and theory.

II. THEORETICAL BASIS

A. Definition of the scattering matrix [*S*] of a discontinuity

The scattering matrix $[S]$ of a discontinuity (in grey in Fig. 1) located between the axial coordinates z_L on side I and z_R on side II (L and R mean, respectively, the left side and right side of the discontinuity) and linked to two waveguides is a linear relationship between the incoming pressure wave

[a]Author to whom correspondence should be addressed; electronic mail: jean-michel.ville@utc.fr

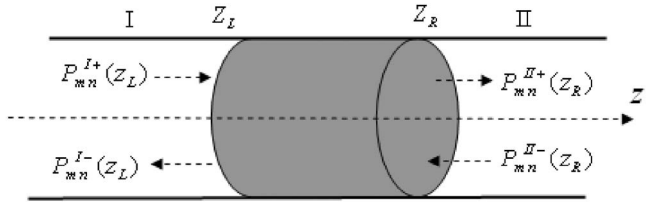

FIG. 1. Waves coming in and out of the discontinuity in gray from sides I and II.

vector $\{P^{\text{in}}\}_{2N}=\{P_{mn}^{\text{I}+}(z_L),P_{mn}^{\text{II}-}(z_R)\}_N^t$ and the outcoming pressure wave vector $\{P^{\text{out}}\}_{2N}=\{P_{mn}^{\text{I}-}(z_L),P_{mn}^{\text{II}+}(z_R)\}_N^t$ where N is the number of modes in both cross sections:[10]

$$\{P^{\text{out}}\}_{2N}=[S]_{2N\times 2N}\times\{P^{\text{in}}\}_{2N} \quad \text{with} \tag{1}$$

$$[S]=\begin{bmatrix}[S^{11}]_{N\times N} & [S^{12}]_{N\times N}\\ [S^{21}]_{N\times N} & [S^{22}]_{N\times N}\end{bmatrix}_{2N\times 2N}.$$

This matrix, which depicts only the discontinuity, is independent of the upstream and downstream acoustic conditions and is filled by $(2N)^2$ coefficients:

$$S_{mn,pq}^{kl}, \quad k,1=1,2 \quad \text{and} \quad m,n,p,q=1,2,\ldots,N.$$

The physical meaning of each elementary matrix is as follows: $[\boldsymbol{S}_{\boldsymbol{mn,pq}}^{\boldsymbol{11}}]_{N\times N}$ is the reflection of the wave coming in the element from the left side; $[\boldsymbol{S}_{\boldsymbol{mn,pq}}^{\boldsymbol{21}}]_{N\times N}$ is the transmission of the wave coming in the element from the left side; $[\boldsymbol{S}_{\boldsymbol{mn,pq}}^{\boldsymbol{22}}]_{N\times N}$ is the reflection of the wave coming in the element from the right side; $[\boldsymbol{S}_{\boldsymbol{mn,pq}}^{\boldsymbol{12}}]_{N\times N}$ is the transmission of the wave coming in the element from the right side.

B. Theory of the procedure to measure the scattering matrix [*S*] of a discontinuity

In no flow conditions, the fluid is assumed to be ideal and linear acoustic theory to be valid. As the discontinuity under test is connected to and between two hard wall cylindrical ducts with radius a (main duct) at axial coordinates z_L and z_R (Fig. 1), the acoustic pressure distribution in the main duct is written[11] in cylindrical coordinates (r,Θ,z) as

$$\boldsymbol{p}(\boldsymbol{r},\theta,\boldsymbol{z},\boldsymbol{t})=\sum_{\boldsymbol{m}=-\infty}^{+\infty}\sum_{\boldsymbol{n}=0}^{\infty}\boldsymbol{P}_{\boldsymbol{mn}}(\boldsymbol{z})\Psi_{\boldsymbol{mn}}^{\boldsymbol{a}}(\boldsymbol{r},\theta)\boldsymbol{e}^{-\boldsymbol{i}\omega\boldsymbol{t}}, \tag{2}$$

where $\Psi_{\boldsymbol{mn}}^{\boldsymbol{a}}(\boldsymbol{r},\theta)=\boldsymbol{J}_{\boldsymbol{m}}(\chi_{\boldsymbol{mn}}/\boldsymbol{a})\boldsymbol{e}^{\boldsymbol{im}\theta}$ are the eigenfunctions; the integers m and n are, respectively, the angular wave number and the radial number ($m=0$, $n=0$ is the plane wave); J_m is the Bessel function of the first kind of order m; χ_{mn}/a is the nth root satisfying the radial hard wall boundary condition on the wall of the main duct $J_m'(\chi_{mn}/a)=0$. The total modal pressure coefficients $P_{mn}(z)$ in the cross sections located at axial coordinates z_L and z_R are given by the following relationship:

$$\boldsymbol{P}_{\boldsymbol{mn}}(\boldsymbol{z})=[\boldsymbol{P}_{\boldsymbol{mn}}^{+}(\boldsymbol{z})+\boldsymbol{P}_{\boldsymbol{mn}}^{-}(\boldsymbol{z})], \tag{3}$$

where pressure waves traveling in the positive and negative z directions are depicted, respectively, in regions I and II by $\boldsymbol{P}_{\boldsymbol{mn}}^{\boldsymbol{I}\pm}(\boldsymbol{z})=\boldsymbol{P}_{\boldsymbol{mn}}^{\boldsymbol{I}\pm}(0)\boldsymbol{e}^{\pm\boldsymbol{ik}_{\boldsymbol{mn}}\boldsymbol{z}}$ and $\boldsymbol{P}_{\boldsymbol{mn}}^{\boldsymbol{II}\pm}(\boldsymbol{z})=\boldsymbol{P}_{\boldsymbol{mn}}^{\boldsymbol{II}\pm}(0)\boldsymbol{e}^{\pm\boldsymbol{ik}_{\boldsymbol{mn}}\boldsymbol{z}}$. $k_{mn}=\sqrt{k^2-(\chi_{mn}/a)^2}$ is the axial wave number of mode (m,n) in the main duct, $k=2\pi f/c_0$, f the frequency, and c_0 the speed of sound in air.

The $(2N)^2$ coefficients of $[S]$ are solutions of the following system deduced from Eq. (1):

$$[S_{mn,pq}^{kl}]_{2N\times 2N}=[P^{\text{out}}]_{2N\times 2N}\times[P^{\text{in}}]_{2N\times 2N}^{-1}. \tag{4}$$

To fill the $2N$ columns of $[P^{\text{out}}]_{2N\times 2N}$ and $[P^{\text{in}}]_{2N\times 2N}$, $2N$ linearly independent modal pressure distributions have to be produced and measured by the experiment in both cross sections located at z_L and z_R and incident and reflected modal pressure waves separated.

III. THE EXPERIMENTAL SETUP AND DATA PROCESSING

The measurement of $[S]$ was carried out with the duct facility built under a grant with E.E.C. during the Ducat program,[12] which was already used to measure reflection and transmission matrices.[9] The pressure distributions measured in two closed cross sections before and after the duct under test by two pairs of microphones are Fourier Lommel's transform[13] then the incident and reflected modes are separated.[9] If N is now the number of cut-on modes, a "selective" computation of the $2N\times 2N$ coefficients of $[S]$ is then performed after a process based on the generation of N independent incident fields for two- or six-load cases depending on the direct or overdetermination procedure is achieved. The load method was chosen instead of the source[7] one because of practical considerations.

A. Hardware

The facility is installed in the anechoic chamber of the University of Technology of Compiegne. The equipment is made of 0.5-m-long duct components with 0.01-m-thick steel wall which all have a 0.148-m internal diameter except of course part of the test duct element. From the left to the right of the schema (Fig. 2) are shown the following elements:

(1) Absorbent element to avoid reflection upstream.
(2) The source section with three acoustic drivers flushed mounted in a z line. The axial distance between two drivers is 0.15 m. All this section can rotate over 360°.
(3) The measurement duct element I which can rotate over 360° is supporting a boom traversing on the radius with a B&K sound intensity probe attached and directed toward the z axis. The distance between the 1/4 in. microphones is 0.054 m according to well-known conditions.[8,13,14]
(4) The 0.5-m-long duct element which will be part of the test configuration.
(5) The measurement duct element II is identical to the duct element I.

Noise is radiated in the anechoic chamber through an unflanged inlet duct which constitutes the load. The different load conditions will be created by changing only the length of this duct. Angular and radial displacements are provided by step by step motors. A working station automatically op-

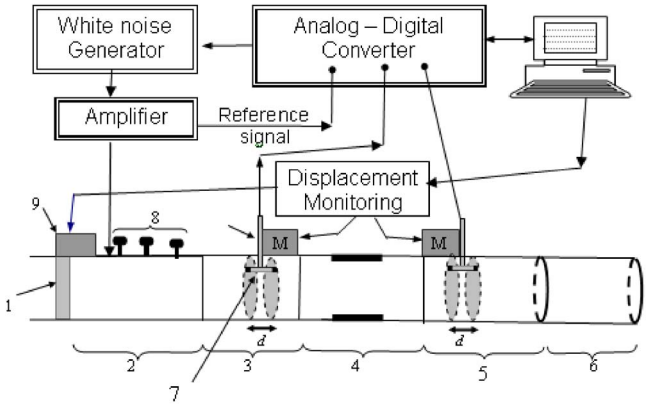

FIG. 2. Experimental setup.

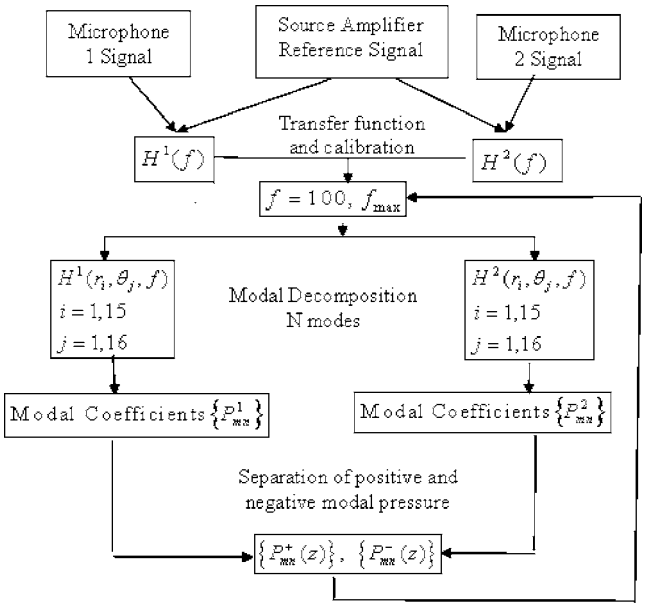

FIG. 3. Flow chart of the data collection in both closed duct sections and separation procedure.

erates the rotation of the source section, the choice of the axial source, and the displacements of the probe in the r and Θ directions. It also supplies the noise generation to sources and the acquisition through an analog-digital converter of the signals issued from the four microphones.

B. The data processing

The experimental procedure is divided into the following steps:

(1) For each load and source configuration:

(a) Collect the frequency spectra of the total modal coefficients in two closed cross sections located in both measurement duct elements.

(b) Separate the incident and reflected modal pressure vectors.

(2) Postprocess the incident and reflected modal pressure vectors on both sides of the test duct element for the N source configurations and two or several loads to get the in and out wave matrices in z_L and z_R.

(3) Compute the scattering matrix.

1. Data collection and reduction

During the first step described in Fig. 3 the acoustic driver is driven with a white noise signal that is band limited to 0–2700 Hz. For this duct radius and frequency range the total adimensional wave number ka is lower than 3.8. Therefore only $N \leqslant 5$ modes (0,0); $(\pm 1, 0)$; $(\pm 2, 0)$ are cut-on. The transfer functions between the amplifier and microphone signals provide, after calibration, the amplitude and phase of the local total acoustic pressure normalized by the level of the amplifier. The origin of the z axis is then given by the reference phase that is in the source z axis position. A 240-point discretization of the acoustic pressure field measured in each of the two pairs of cross-section areas is achieved by rotating the measurement duct section at 16 positions equally spaced by 22.5° and displacing the probe to 15 radial positions. Then modal decomposition by a Fourier-Lommel's transform[8,13] for $m=-7$ to $+7$ and $n=0$ to 3 is achieved leading to the cut-on or cut-off complex modal pressure coefficients in both pairs of cross-section areas. The incident and reflected modal vectors are then separated and computed at z_L and z_R.

All this procedure is repeated for all source configurations and loads. To compute the 100 coefficients of the matrix $[S]$, at least 10 experiments (5 source configurations and 2 loads) have to be performed. The 5 source configurations and loads have been chosen[8] to ensure generation of linearly independent input modal vectors. The coordinates of the source and the characteristics of the loads used are given in Table I.

2. Data postprocessing (Fig. 4)

At the end of the first step the modal coefficient vectors $\{P_{mn}^{\mathrm{I}+}(z_L)\}\{P_{mn}^{\mathrm{II}+}(z_R)\}$ of the positive waves and $\{P_{mn}^{\mathrm{I}-}(z_L)\} \times \{P_{mn}^{\mathrm{II}-}(z_R)\}$ of the negative waves are available at each side of the discontinuity for each source and load configurations and the matrices $[P^{\mathrm{in}}]_{2N\times 2N}$ and $[P^{\mathrm{out}}]_{2N\times 2N}$ are filled. The scattering matrix is then deduced from the relationship Eq. (4) during the second step as shown in Fig. 4.

Equation (4) can be solved in two ways:

(1) With the "selective" method, the rank of $[S]$ is linked to the number of cut-on modes and will then depend upon the frequency. Only the propagating modes are taken into account assuming that the influence of the cut-off modes can be neglected.

(2) With the "global" method, the rank of $[S]$ is constant being independent of the frequency and fixed in relation to the higher limit of the frequency band studied, i.e., 2700 Hz, $N=5$ and the rank of $[S]=100$ in our experiment. The overall modal basis is considered including the nonpropagating modes.

TABLE I. Coordinates of the source and length of the load configurations.

Configuration No.	Angular position $\theta_S^i(^\circ)$ of the source	Axial position z_S^i (cm) of the source	Length of the load E (cm)
1	0	0	0
2	120	+15	3
3	240	−15	6
4	8.5	0	9
5	128.5	+15	12
6	248.5	−15	18
7	17	0	0
8	137	+15	3
9	257	−15	6
10	25.5	0	9
11	145.5	+15	12
12	265.5	−15	18
13	34	0	0
14	154	+15	3
15	274	−15	6
16	42.5	0	9
17	162.5	+15	12
18	282.5	−15	18
19	51	0	0
20	171	+15	3
21	291	−15	6
22	59.5	0	9
23	179.5	+15	12
24	299.5	−15	18
25	68	0	0
26	188	+15	3
27	308	−15	6
28	76.5	0	9
29	196.5	+15	12
30	316.5	−15	18

Later on in this paper (Sec. V C 2), the experimental results of the calculation of a $[S]$ coefficient (Fig. 19) deduced from both techniques will be compared and show they provide nearly the same result. Therefore the "selective" method has been chosen to solve Eq. (4). It is well known that this direct method based upon the inversion of the $[P^{\text{in}}]_{2N\times 2N}$ matrix [Eq. (4)] leads to numerical problems. To avoid this difficulty an overdetermination technique[15,16] often used to solve a system where the number of equations $L\times N$ $(L>2)$ is higher than $2N$ the number of unknowns was developed. The scattering matrix $[S]$ is then now deduced from the relationship:[17]

$$[S]^T_{2N\times 2N} = [[^*[P^{\text{in}}]_{2N\times(L\times N)} \times [P^{\text{in}}]^T_{2N\times(L\times N)}]^{-1} \times {}^*[P^{\text{in}}]_{2N\times(L\times N)}] \cdot [P^{\text{out}}]^T_{2N\times(L\times N)}. \quad (5)$$

The columns of the rectangular matrices $[P^{\text{in}}]_{2N\times(L\times N)}$ and $[P^{\text{out}}]_{2N\times(L\times N)}$ are filled by repeating N experiments associated to N source configurations for L=4 or 6 load configurations ensuring[8] again that the $L\times N$ pressure distributions are linearly independent.

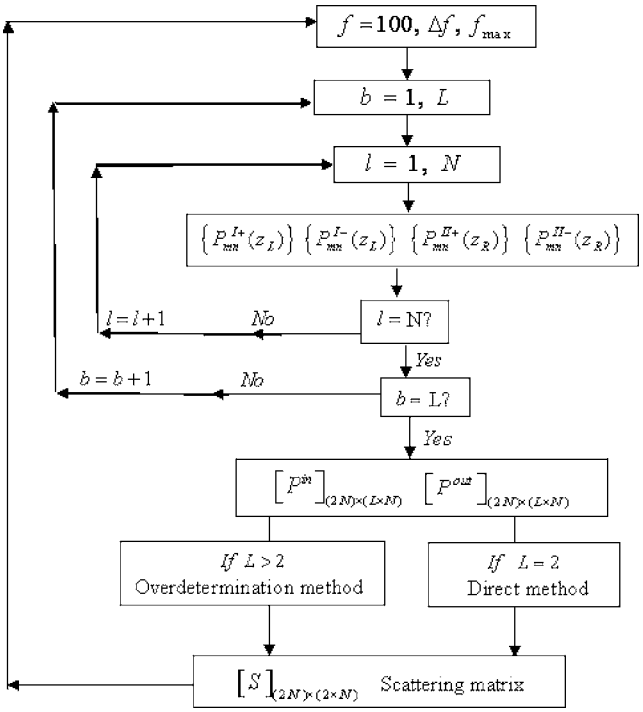

FIG. 4. Flow chart of the scattering matrix coefficients calculation.

C. The configurations tested

The axial positions z_R and z_L defined in Fig. 1 correspond, respectively, to the axial coordinates of the two microphones located on each side of the duct under test. Then the duct element for which the scattering matrix is measured is 1 m long including the 0.5-m-long test duct and parts of the measurement ducts. The two discontinuities tested are symmetrical in relation to the duct axis and to the axial centerline. The first configuration is a 0.5-m-long element duct which is identical to the other elements. It has been chosen to become a reference test because its theoretical scattering matrix is well known (Appendix B) and also because the experimental conditions are more favorable with respect to the stationary wave problem. The second configuration is a reactive type chamber shown in Fig. 5 which introduces more complicated measurement conditions. It is made with the reference 0.5-m-long straight duct in which a 5.5-cm-diam axisymmetric cylindrical duct is mounted.

IV. ANALYSIS OF THE EXPERIMENTAL RESULTS

To analyze the experimental results several theoretical developments have been achieved:

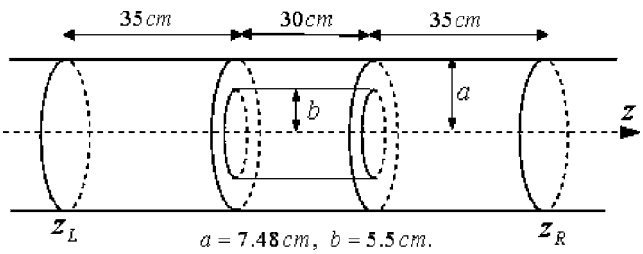

FIG. 5. The reactive muffler located between z_L and z_R.

(1) A theoretical calculation of $[S]$ for both configurations which the experimental results are compared with.
(2) An analytical simulation of the experiment and an error calculation on the determination of $\{P^{I+}_{mn}(z_L)\}$ and $\{P^{I-}_{mn}(z_L)\}$ by the separation procedure to discuss the discrepancies between experiment and theory.

Among the $(2N)^2=100$ coefficients ($N=5$) of $[S]$ only typical results for the plane wave and for higher order modes $m=1$ and 2 are presented emphasizing the symmetry properties of both discontinuities.

A. Influence of errors

The resulting error on the calculation of $[S]$ will depend on two things: (1) the errors in the input measured data, i.e., temperature, transfer functions, and position of the microphones; and (2) the sensivity to errors in the input data of the calculation formulas, i.e., induct modal decomposition, incident and reflected waves separation, and calculation of $[S]$.

During a previous study[14] on the influence of errors on the two-microphone separation method assuming plane wave propagation condition, some practical conclusions about the overall length of the duct, the reflective conditions on the source and open end sides were drawn in order to keep error in the transfer function estimate at 1% in the magnitude and 0.6° in phase. Also as a result of this study, a condition on the distance d between microphones which has to be respected in order to avoid a very large sensitivity to errors in input data during the separation procedure was deduced. In our experiment this distance d was chosen equal to 5.4 cm in order to respect this condition leading to an upper frequency limit of 2700 Hz (Sec. III A). For higher order mode propagation conditions, the sensitivity to the modal decomposition technique in the microphone location and signal to noise ratio was already discussed during previous works.[18] Assuming the technique to be a generalization of this developed for plane wave case[8,19] the optimal distance of separation was extended to higher order mode propagation conditions.

The calculation of error presented in this paper based upon a direct simulation of the experiment described in the following begins by the separation procedure and includes the calculation of $[S]$, then excluding the sensitivity to errors in the input data to the modal decomposition stage which is therefore considered as a known input data to the simulation program as shown in Fig. 6. Moreover, an analytical calculation of the error produced by the separation process based on a first-order Taylor expansion of the calculation formulas is presented in Appendix D. Results of this study will emphasize for higher order mode propagation condition the high sensitivity of this step to errors in input data such as temperature and total modal pressure when the frequency becomes very close to the cut-off mode frequency while for the plane wave the sensitivity to the error on temperature can be neglected compared to the error on total modal pressure.[20]

Another effect to be considered is the influence from the nonpropagating mode on the measurement of $[S]$. According to a study which discusses this matter for the plane wave case[14] the microphones should not be placed closer than about 10 mm from the discontinuity or a sample to avoid the

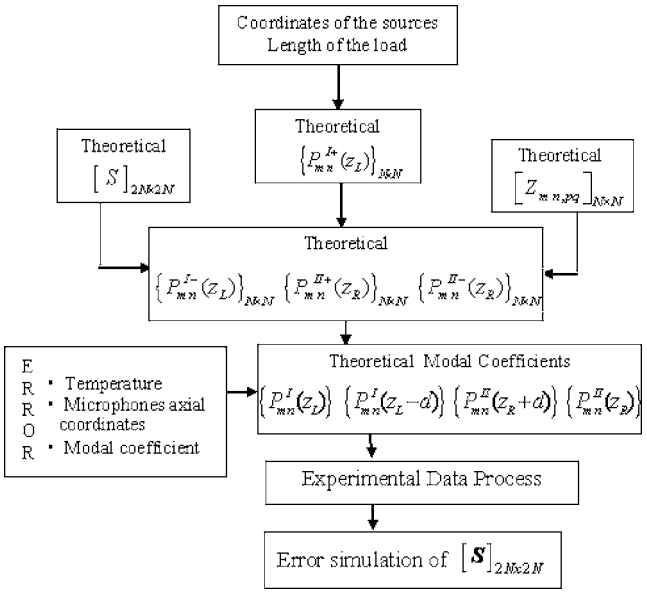

FIG. 6. Flow chart of the error estimation by a simulation process of the experiment.

effect of near field. For higher order mode propagation condition when the frequency approaches the cut-off frequency the influence of the evanescent mode increases as the "damping" length becomes long. In the present study the modal basis which the decomposition technique is calculated with, includes all modes up to $m=\pm 7$, $n=3$ whatever the frequency is (Sec. III B 1) avoiding the influence of the evanescent modes up to the separation step included in the frequency band studied. Another problem is to include in the calculation of the matrix $[S]$ the conversion coefficients in reflection and transmission from a cut-on mode to a cut-off mode which assumes the modal basis used in Eq. (4) is extended to the nonpropagating modes. It will be shown in Sec. V C 2 that for an axisymmetric discontinuity in the frequency domain down to the cutoff frequency of the $(0,1)$ and as the distance between the discontinuity and the measurement cross section is far enough, the influence of the evanescent modes can be neglected. This assumption was already verified in previous studies where reflection and transmission matrices were measured.[8,9]

Then the direct simulation program has provided the calculation of error produced through the matrix scattering formulas for a 5° error on temperature and (1°, 5%) error on, respectively, the phase and the amplitude of the total modal pressure coefficients measured in both cross section values assumed to be representative of a real measurement situation.

B. Theoretical simulation of the experiment

1. Theory of the simulation

Figure 7 shows the duct arrangement used to simulate the experiment. It is made of the duct element located between z_L and z_R and defined by its theoretical scattering matrix $[S]$. On the left side of this duct element a semi-infinite duct is supporting the source section and on the right side a finite length duct is radiating outside through an infinite baffled open end. The total pressures in the four cross sections where the microphones are located are then calculated

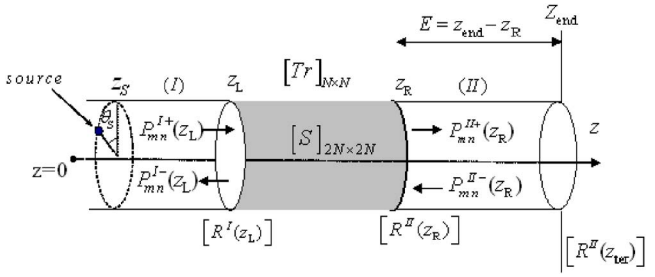

FIG. 7. Duct configuration of the simulation process.

analytically for each source and load configuration listed in Table I. To perform this simulation the following analytical calculations have to be carried out:

(1) The scattering matrix $[S]$ (Appendices A and B).
(2) The impedance matrix $[\boldsymbol{Z_{mn,pq}}]_{N\times N}$ of the open end reflection.[19]
(3) The incident pressure matrix in the semi-infinite duct $\{\boldsymbol{P_{mn}^{I+}}(z_L)\}_{N\times N}$ deduced for each of the N source configurations (Table I) assuming a point source defined by its amplitude $A_s=1$ and phase $\varphi_s=0$ and located at (z_s,θ_s,a).
(4) The modal pressure coefficients in both duct cross-section areas for all sources and loads configurations given in Table I (Appendix C).

2. The simulation procedure

The flow chart of the simulation procedure is described in Fig. 6. Its validation was carried out by introducing the theoretical values of $[S]$ and verifying that when no errors are assumed the procedure results in the same matrix $[S]$. The sensitivity of $[S]$ to errors on the following parameters were then studied by introducing errors on the temperature, modulus and phase of the modal pressure coefficients, and axial positions of the microphones.

C. Experimental results

1. Straight duct

Influence of the number of loads on the experimental results. The advantage of the overdetermination procedure over the direct method is clear in Fig. 8 where the variations of the transmission coefficient of the plane wave $S_{00,00}^{1,2}$ vs ka for two and six loads are compared with theory. All "instabilities" in the high frequency domain have been avoided when the overdetermination method is performed. As a consequence, all other results presented in the paper were carried out with the overdetermination method with six loads.

Analysis of some $[S]$ *coefficients.* The modulus of the transmission coefficients $[S_{00,00}^{1,2};S_{00,00}^{2,1}]$ and reflection ones $[S_{00,00}^{1,1};S_{00,00}^{2,2}]$ for the plane wave $(0,0)$ coming in the discontinuity from the left and right sides respectively, are plotted versus ka up to 3.8 and compared to the analytical results in Fig. 9. In Fig. 10 the same results are presented for the higher order mode case $(-1,0)$. At once the three following comments have to be made:

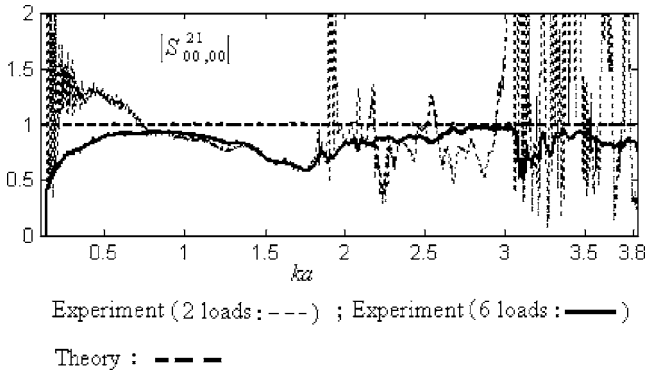

FIG. 8. Comparison with theory for the straight duct configuration of $|S_{00,00}^{2,1}|$, the experimental transmission coefficient vs ka of the plane wave mode traveling from the left to the right side deduced from the direct and overdetermination methods.

(1) The experimental curves $S_{m0,m0}^{2,1}$, $S_{m0,m0}^{1,1}$ are nearly superimposed on, respectively, $S_{m0,m0}^{1,2}$, $S_{m0,m0}^{2,2}$ for $m=0,-1$ verifying the symmetry property of the element with respect to its median plan.
(2) The experiment underestimates the theoretical transmission coefficients for both modes near the cut-off frequency, for $1.5<ka<2$ and for ka close to 3. Also a slow increase with frequency from 0 at the cut-off frequency to 1 instead of the step function predicted by theory is evident for $m=-1$.
(3) The experimental reflection coefficients oscillate between 0 and 0.2 reaching higher values near cut-off frequencies in opposite to the theory which predicts no reflection.

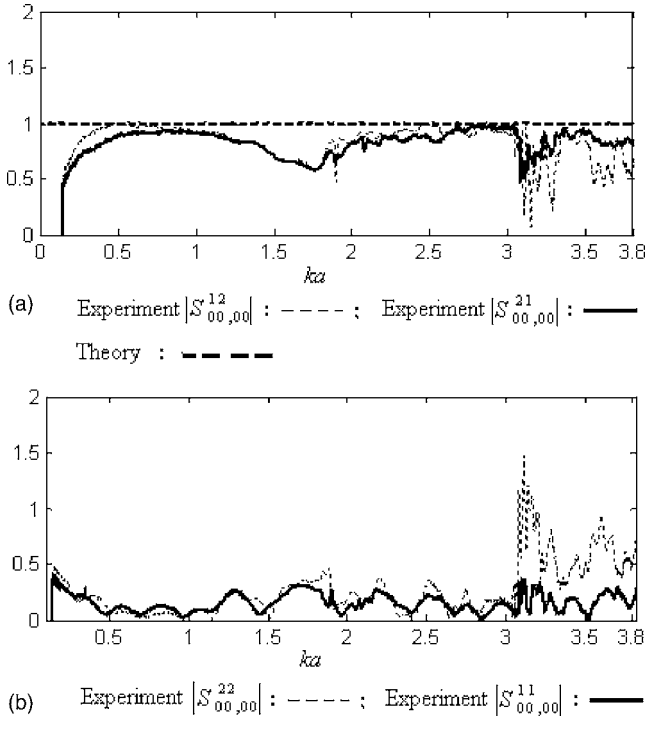

FIG. 9. Comparison with theory for the straight duct configuration of: (a) $|S_{00,00}^{2,1}|$ and $|S_{00,00}^{1,2}|$ the experimental transmission coefficients vs ka of the plane wave mode traveling, respectively, from the left to the right side and from the right to the left side; (b) $|S_{00,00}^{1,1}|$ and $|S_{00,00}^{2,2}|$ the experimental reflection coefficients vs ka of plane wave mode coming in the straight duct from the left side and from the right side, respectively.

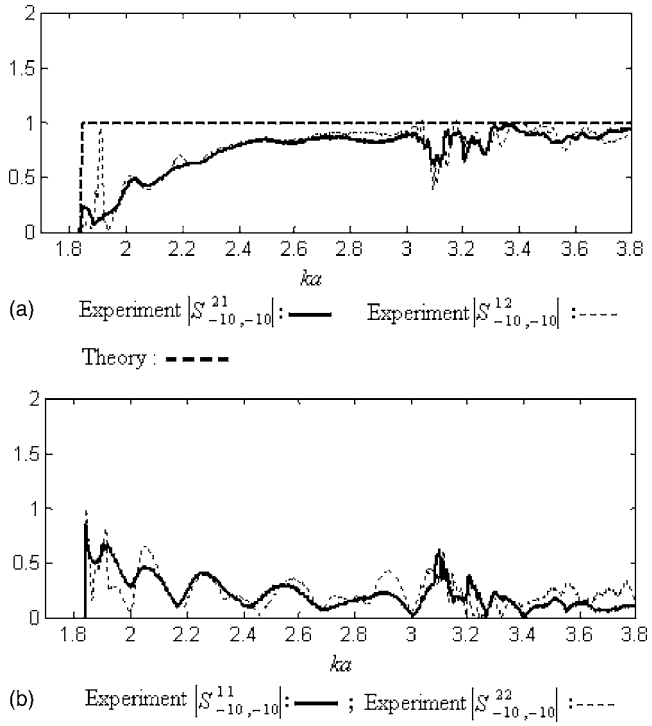

FIG. 10. For the straight duct configuration: (a) Comparison with theory of $|S^{2,1}_{-10,-10}|$ and $|S^{1,2}_{-10,-10}|$ the transmission coefficients vs ka of mode $(-1,0)$ traveling, respectively, from the left to the right side and from the right to the left side; (b) $|S^{1,1}_{-10,-10}|$ and $|S^{2,2}_{-10,-10}|$ the experimental reflection coefficients vs ka of mode $(-1,0)$ coming in the straight duct from the left side and from the right side, respectively.

The effect on the coefficients $S^{2,1}_{-10,-10}$ and $S^{1,1}_{-10,-10}$ of a 5° discrepancy on temperature and $(1°,5\%)$ error on, respectively, the phase and the amplitude of modal pressure coefficients in two of the cross-section areas was estimated with the simulation procedure. In Fig. 11 the comparison between simulated and experimental results points out that these coefficients are very sensitive to errors but only in the frequency domain very close to the cut-off mode frequency. In Appendix D, this influence is shown to come from the sensitivity of the separation procedure in the input data such as temperature and total modal pressure explaining only part of the difference between experiment and theory. Indeed the periodic oscillation on the reflection coefficient and the slow variation of the transmission coefficient noticed before on mode $m=-1$ are not due to errors but caused by a physical phenomenon which is probably, as justified in the following, produced by a vibration of the duct wall. Indeed, the step variation of the theoretical transmission coefficient at the cut-off frequency and the nonreflection assume that the normal velocity on the wall is zero. But it is well known that this condition is not realistic and a coupling between acoustic duct cavity and duct wall vibration always occurs and can become stronger particularly when the frequency approaches by upper values the mode cut-off frequency.

Typical experimental results of the conversion coefficients of mode $m=-1$ into $m=0$ in transmission and reflection for waves coming in the discontinuity from the left and the right sides, respectively, are plotted in Fig. 12. All coefficients are lower than 0.1 except near the cut-off frequencies of modes. This result verifies the property of axisymmetry of the element which leads theoretically to no conversion between angular modes. Moreover, the couples of curves

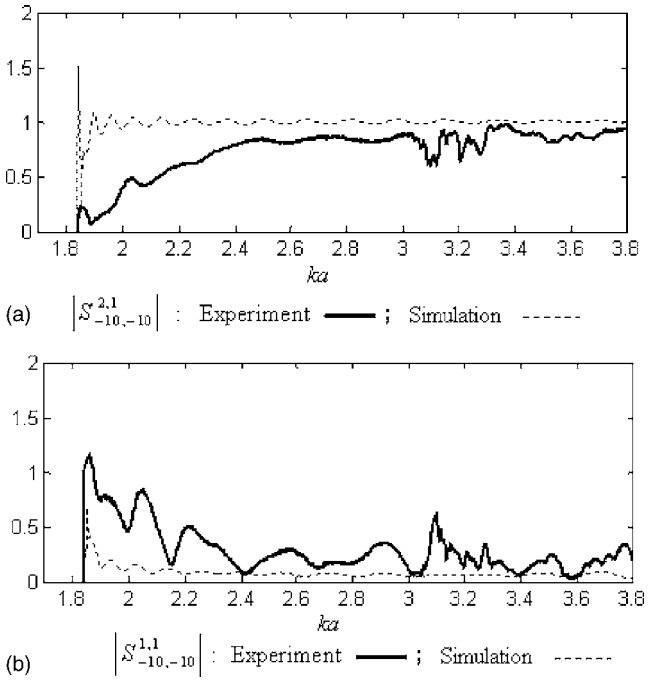

FIG. 11. For the straight duct configuration comparison between experiment and simulation with a 5° error on temperature and $(1°,5\%)$ errors on, respectively, the phase and the amplitude of the modal pressure coefficient: (a) $|S^{2,1}_{-10,-10}|$ the transmission coefficient vs ka and (b) $|S^{1,1}_{-10,-10}|$ the reflection coefficient vs ka.

$[S^{2,1}_{00,-10};S^{1,2}_{00,-10}]$ and $[S^{1,1}_{00,-10};S^{2,2}_{00,-10}]$ are nearly superimposed verifying the assumption of symmetry of the element with respect to its median plan.

2. The Chamber

The modulus of the transmission coefficients $[S^{1,2}_{mn,mn};S^{2,1}_{mn,mn}]$ and reflection coefficients $[S^{2,2}_{mn,mn};S^{1,1}_{mn,mn}]$

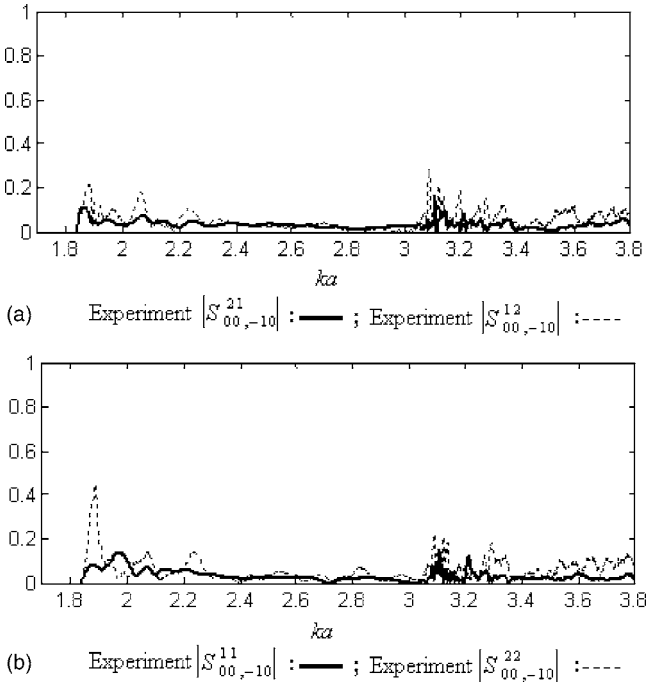

FIG. 12. For the straight duct configuration the experimental conversion coefficients of mode $(-1,0)$ into $(0,0)$ vs ka: (a) $|S^{2,1}_{00,-10}|$ and $|S^{1,2}_{00,-10}|$ in transmission; (b) $|S^{1,1}_{00,-10}|$ and $|S^{2,2}_{00,-10}|$ in reflection.

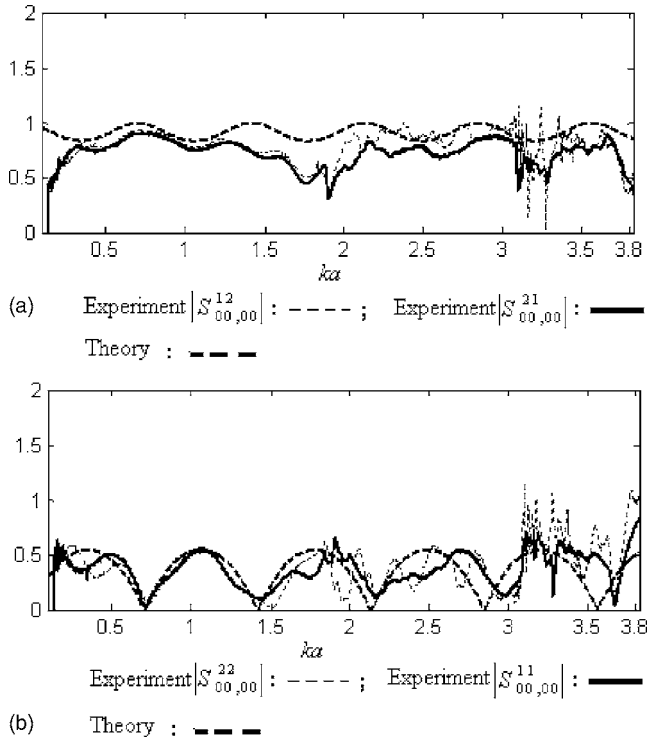

FIG. 13. Comparison for the reactive duct configuration between theory and experiment of: (a) $|S^{2,1}_{00,00}|$ and $|S^{1,2}_{00,00}|$ the transmission coefficients vs ka of mode (0,0) traveling, respectively, from the left to the right side and from the right to the left side; (b) $|S^{1,1}_{00,00}|$ and $|S^{2,2}_{00,00}|$ the reflection coefficients of mode (0,0) coming in the element, respectively, from the left side and from the right side.

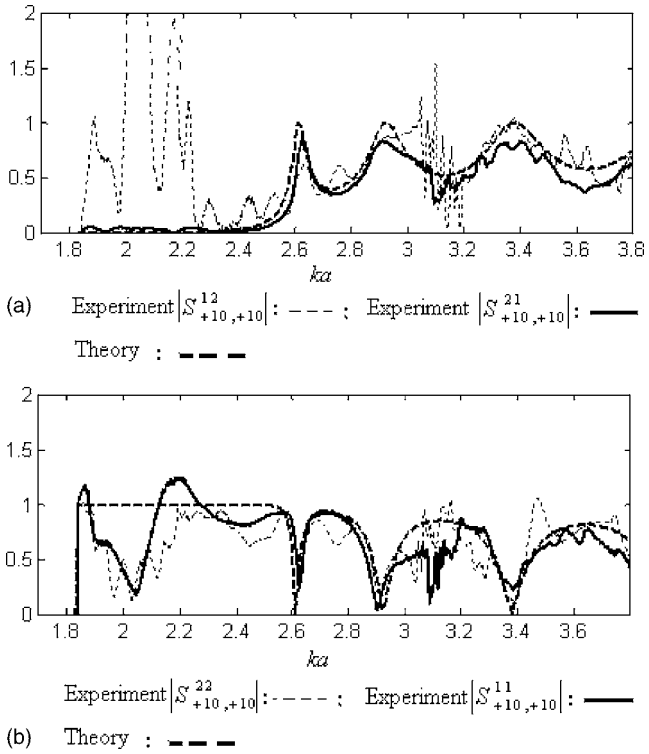

FIG. 14. Comparison for the reactive duct configuration between theory and experiment of: (a) $|S^{2,1}_{+10,+10}|$ and $|S^{1,2}_{+10,+10}|$ the transmission coefficients vs ka of mode (+1,0) traveling, respectively, from the left to the right side and from the right to the left side; (b) $|S^{1,1}_{+10,+10}|$ and $|S^{2,2}_{+10,+10}|$ the reflection coefficients vs ka of mode (+1,0) coming in the element from the left side and from the right side, respectively.

through the duct element which contains the chamber for waves traveling from the left and the right sides are plotted for $m=0$, 1, and 2 and compared to the analytical results in Figs. 13, 14, and 16, respectively.

For the plane wave $m=0$ (Fig. 13) the agreement between experiment and theory is good but some differences have to be noticed:

(1) For $1.5<ka<2$ and around $ka=3$ the experimental transmission coefficient is smaller than the theoretical one as already observed before with the straight element and justified by a vibroacoustic coupling.
(2) The symmetry of the discontinuity with respect to its median plan is verified for $ka<2$. The small diameter duct is filtering the pressure distributed on mode $m=1$ for $1.8<ka<2.51$ and $m=2$ for $3.05<ka<4.16$ (Table II) leading to a worse signal to noise ratio downstream of the chamber and then noisier coefficients $S^{1,2}_{00,00}$ and $S^{2,2}_{00,00}$ for waves traveling from the right to the left.
(3) Just below $ka=3.8$ the cut-off frequency of the mode (0,1) the shift between experimental and theoretical minima and maxima is produced because the conversion of mode (0,1) into (0,0) is not taken into account by the analytical model.

The incident pressure $\boldsymbol{P}^{I+}_{10}(z)$ on mode $m=1$ on the source side is filtered by the chamber for $1.84<ka<2.51$ (Table II). Then in the analysis to follow the results associated to the waves traveling from the left and right sides of the chamber are discussed separately. Indeed Fig. 14 points out the following:

(1) $S^{2,1}_{10,10}$ and $S^{1,1}_{10,10}$, the transmission and reflection coefficients for waves traveling from the left to the right, agree well with the theory.
(2) For ka up to 2.51 as $\boldsymbol{P}^{I+}_{10}(z)$ is filtered by the chamber, on the open side the pressure level is very low. The measurements of both coefficients $S^{1,2}_{10,10}$ and $S^{2,2}_{10,10}$ are based on the incoming wave traveling from the right side of the chamber. This pressure wave results from the reflection by the duct inlet of the wave which was already transmitted through the chamber. The pressure coming out on the left side of the chamber which is used to measure $S^{1,2}_{10,10}$ has then been filtered two times. This explains why in this frequency domain the signal to noise ratio becomes so low that such an important discrepancy occurs between experiment and theory and also why this error is more important on the transmission coefficient than on the reflection one. This effect is well reproduced (Fig. 15) by the simulation of the experiment where it was assumed a 5° discrepancy on temperature and 1°, 5% on,

TABLE II. Cut-off ka frequencies of duct with radius a and b.

(m,n)	ka (a=7.48 cm)	ka (b=5.5 cm)
(0,0)	0	0
(±1,0)	1.8412	2.51
(±2,0)	3.0542	4.16

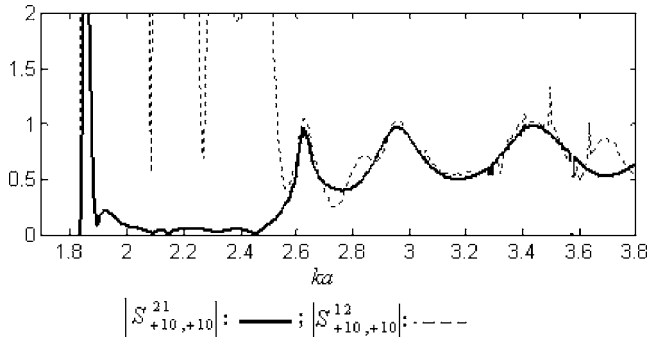

FIG. 15. For the reactive duct configuration simulation of $|S^{2,1}_{+10,+10}|$ and $|S^{1,2}_{+10,+10}|$ the transmission coefficients vs *ka* of mode (+1,0) with a 5° error on temperature and (1°,5%) error on, respectively, the phase and the amplitude of the modal pressure coefficients.

respectively, the phase and the amplitude of modal pressure coefficients in the two cross sections. This result emphasizes also that the measurement of this coefficient in this propagation condition is very sensitive to errors on the experimental parameters.

(3) For $ka > 2.51$ the symmetry of the discontinuity with respect to its median plan is verified even for the plane wave case because the coefficients which are associated to the waves traveling from the right to the left are noisier than those traveling from the left to the right.

The incident pressure distributed on mode (2,0) is cut-off by the chamber for all the *ka* spectrum studied (Table II). The interpretation of the experimental results (Fig. 16) developed for the mode (1,0) when it is cut-off has to be extended for the (2,0) mode to all *ka* studied. Indeed the transmission coefficient $S^{2,1}_{20,20}$ and the reflection one $S^{1,1}_{20,20}$ related to the wave traveling from the left to the right agree with theory. But the measurement of $S^{1,2}_{20,20}$ transmission coefficient resulting from the wave traveling from the right to the left is completely wrong while the reflection coefficient $S^{2,2}_{20,20}$ is better determined allowing one to verify the symmetry of the discontinuity with respect to the chamber median plan.

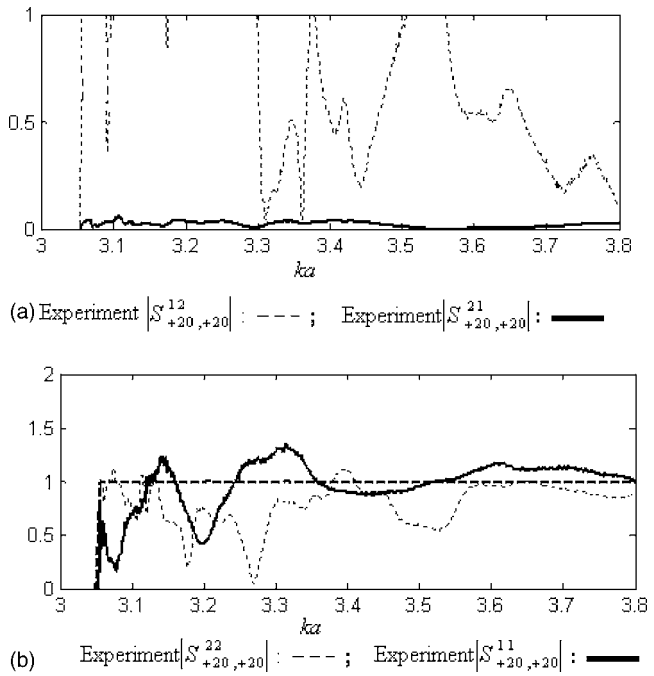

FIG. 16. Comparison for the reactive duct configuration with theory of: (a) $|S^{2,1}_{+20,+20}|$ and $|S^{1,2}_{+20,+20}|$ the experimental transmission coefficients vs *ka* of mode (+2,0), respectively, from the left to the right side and from the right to the left side; (b) $|S^{1,1}_{+20,+20}|$ and $|S^{2,2}_{+10,+10}|$ the experimental reflection coefficients vs *ka* of mode (+2,0) coming in the element from the left side and from the right side, respectively.

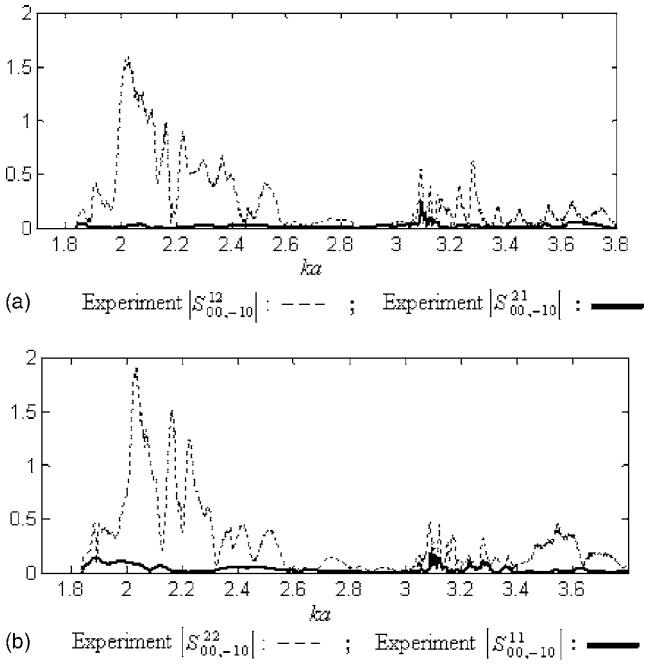

FIG. 17. For the reactive duct configuration, experimental conversion coefficients vs *ka* for mode (−1,0) into (0,0): (a) $|S^{2,1}_{00,-10}|$ and $|S^{1,2}_{00,-10}|$ transmission, respectively, from the left to the right side and from the right to the left side; (b) $|S^{1,1}_{00,-10}|$ and $|S^{2,2}_{00,-10}|$ reflection coming in the element from the left side and from the right side, respectively.

In Fig. 17 are plotted conversion coefficients in transmission and reflection of the mode (−1,0) into the plane wave. Again the coefficients agree with theory, which predicts a zero value because of the axisymmetry of the geometry but only for the wave traveling from the left to the right. The computation by the simulation program of the conversion coefficients in reflection with errors on temperature and modal coefficients reproduces the experimental curves as shown in Fig. 18, verifying the high sensitivity of this measurement to uncertainties.

In Fig. 19, the results of the measurement of $|S^{2,1}_{10,10}|$, the modulus of the transmission coefficient versus *ka* already presented in Fig. 14, are compared with the results deduced when the modal basis used for the calculation of $[S]$ includes all five modes in the complete frequency domain meaning that the influence of the evanescent mode is taken into account. As both curves are superimposed, we can deduce that in our test configuration the nonpropagating modes can be neglected.

V. CONCLUSIONS

An experimental procedure was achieved to measure the scattering matrix of a duct discontinuity for higher order mode propagation conditions. Straight and reactive type silencer duct configurations were tested and the experimental

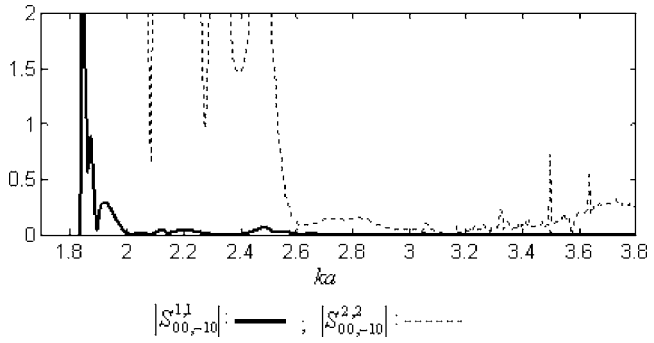

FIG. 18. For the reactive duct configuration, simulation with a 5° error on temperature and (1°,5%) errors on, respectively, the phase and the amplitude of the modal pressure coefficients of $|S^{1,1}_{00,-10}|$ and $|S^{2,2}_{00,-10}|$ the conversion coefficients vs *ka* in reflection for mode (−1,0) into (0,0) respectively coming in the element from the left side and from the right side.

results compared with theory. The analysis of the results performed mode per mode on the straight configuration showed that the overdetermination procedure with six loads improves the results. An analytical procedure of the experiment was developed and used to point out the sensitivity of the experimental parameters errors on $[S]$ measurements. Indeed, it was shown to be important but localized very near the mode cut-off frequency. The other differences between theoretical and experimental variations of the transmission and reflection coefficients are explained by the assumption of the nonrealistic theoretical hard duct wall condition. The symmetry properties of the straight duct geometry with respect to the duct axis and its medium plan were verified experimentally.

The experiment with the reactive chamber has pointed out the filtering effect of a reduction of the diameter of the duct on acoustic modal propagation. Experimental and theoretical results agree in the frequency domain where the modes are cut-on in all test configurations. When the modes are cut-off by the smaller diameter duct the experimental results associated to the incident wave coming from the source side also agree with theory. But the method is unable to measure $[S]$, especially the transmission coefficient associated to the wave traveling from the open end side in this frequency domain. The simulation also shows that, in these conditions, the method is very sensitive to errors leading clearly to wrong results. When the discontinuity is not symmetric with respect to its middle plan, the two source technique or a permutation of the chamber has to be applied to improve the results.

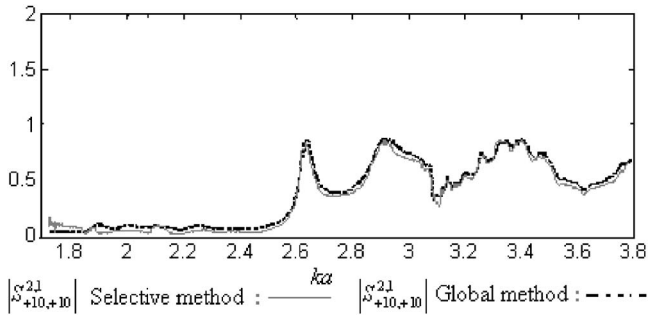

FIG. 19. For the reactive duct configuration experimental $|S^{2,1}_{+10,+10}|$ the transmission coefficient vs *ka* of mode (+1,0) traveling from the left to the right side deduced from selective and global methods.

APPENDIX A: CALCULATION OF THE SCATTERING MATRIX FROM A GIVEN TRANSFER MATRIX

The transfer matrix $[T]_{N\times N}$ of a duct element like this shown in Fig. 1 is defined by

$$\begin{Bmatrix} P^{\mathrm{II}} \\ V_z^{\mathrm{II}} \end{Bmatrix}_{2N} = [T]_{2N\times 2N} \times \begin{Bmatrix} P^{\mathrm{I}} \\ V_z^{\mathrm{I}} \end{Bmatrix}_{2N}. \tag{A1}$$

P and V_z are, respectively, the total pressure and the axial acoustic particle velocity vectors expressed versus their modal description by

$$\{P^{\mathrm{I}}, V_z^{\mathrm{I}}\}_{2N} = \{P^{\mathrm{I}}_{mn}(z_L), V^{\mathrm{I}}_{z,mn}(z_L)\}^t_N, \tag{A2}$$

$$\{P^{\mathrm{II}}, V_z^{\mathrm{II}}\}_{2N} = \{P^{\mathrm{II}}_{mn}(z_R), V^{\mathrm{II}}_{z,mn}(z_R)\}^t_N.$$

It is well known that the axial acoustic particle velocity is deduced from the pressure by[1]

$$V_{z,mn}(z) = Y^a_{mn}(P^+_{mn}(z) - P^-_{mn}(z)) \tag{A3}$$

with $Y^a_{mn} = (k^a_{mn}/\rho_0 c_0 k)$.

Developing Eq. (A1) and replacing these total acoustic quantities versus the incident (+) and reflected (−) pressure and axial particle velocities two relationships are deduced:

$$\{P^{\mathrm{II}+}_{mn}(z_R)\}_N + \{P^{\mathrm{II}-}_{mn}(z_R)\}_N = [X^+]_{N\times N} \cdot \{P^{\mathrm{I}+}_{pq}(z_L)\}_N + [X^-]_{N\times N} \cdot \{P^{\mathrm{I}-}_{pq}(z_L)\}_N, \tag{A4}$$

$$\{P^{\mathrm{II}+}_{mn}(z_R)\}_N - \{P^{\mathrm{II}-}_{mn}(z_R)\}_N = [W^+]_{N\times N} \cdot \{P^{\mathrm{I}+}_{pq}(z_L)\}_N + [W^-]_{N\times N} \cdot \{P^{\mathrm{I}-}_{pq}(z_L)\}_N, \tag{A5}$$

where

$$[X^\pm]_{N\times N} = ([T^{11}]_{N\times N} \pm [\mathrm{diag}(Y^a_{mn})]_{N\times N} \cdot [T^{12}]_{N\times N}), \tag{A6}$$

$$[W^\pm]_{N\times N} = [\mathrm{diag}(Y^a_{mn})]^{-1}_{N\times N} \cdot ([T^{21}]_{N\times N} \pm [\mathrm{diag}(Y^a_{mn})]_{N\times N} \cdot [T^{22}]_{N\times N}). \tag{A7}$$

As the scattering matrix is given by Eq. (1) and using Eqs. (A5) and (A6) the expressions of the four elementary matrices of $[S]$ vs $[X^\pm]_{N\times N}$ and $[W^\pm]_{N\times N}$ are deduced:

$$[S^{1,1}]_{N\times N} = [[[X^-]_{N\times N} - [W^-]_{N\times N}]^{-1} \cdot ([W^+]_{N\times N} - [X^+]_{N\times N})]_{N\times N}, \tag{A8}$$

$$[S^{1,2}]_{N\times N} = 2[[X^-]_{N\times N} - [W^-]_{N\times N}]^{-1}_{N\times N}, \tag{A9}$$

$$[S^{2,2}]_{N\times N} = [-[[X^-]^{-1}_{N\times N} - [W^-]^{-1}_{N\times N}]^{-1} \cdot ([X^-]^{-1}_{N\times N} + [W^-]^{-1}_{N\times N})]_{N\times N}, \tag{A10}$$

$$[S^{2,1}]_{N\times N} = [[[X^-]^{-1}_{N\times N} - [W^-]^{-1}_{N\times N}]^{-1} \cdot ([X^-]^{-1}_{N\times N} \cdot [X^+]_{N\times N} - [W^-]^{-1}_{N\times N} \cdot [W^+]_{N\times N})]_{N\times N}. \tag{A11}$$

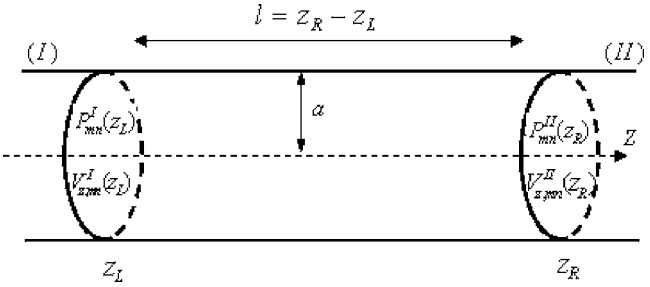

FIG. 20. Schema of the straight duct configuration.

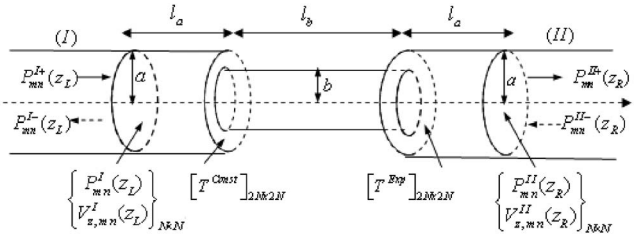

FIG. 21. Schema of the reactive chamber configuration.

APPENDIX B: CALCULATION OF THE TRANSFER MATRICES OF THE STRAIGHT DUCT AND OF THE REACTIVE CHAMBER CONFIGURATIONS

The scattering matrices of both configurations are deduced from their transfer matrices using the relationships given in Appendix A. Then in the following paragraphs only the transfer matrices of both configurations are calculated.

The straight duct (Fig. 20). If N modes are cut-on in a straight duct with radius a located between z_L and z_R, its transfer matrix is defined[1] also by Eqs. (A1) and (A2). If $V_{z,mn}(z)$ is given by Eq. (A3), the transfer matrix of a straight element of radius a and length l is[1]

$$[T_{a,l}]_{2N\times 2N} = \begin{bmatrix} [\mathrm{diag}(\cos(k^a_{mn}l)]_{N\times N} & [\mathrm{diag}((i/Y^a_{mn})\cdot\sin(k^a_{mn}l)]_{N\times N} \\ [\mathrm{diag}(iY^a_{mn}\cdot\sin(k^a_{mn}l)]_{N\times N} & [\mathrm{diag}(\cos(k^a_{mn}l)]_{N\times N} \end{bmatrix}_{2N\times 2N}. \tag{B1}$$

Reactive muffler (Fig. 21). If N modes are cut-on in the main duct with radius a, the transfer matrix of the duct element located between z_L and z_R is deduced by

$$[T]_{2N\times 2N} = [T_{a,l_a}]_{2N\times 2N}[T^{\mathrm{Const}}]_{2N\times 2N} \times [T_{b,l_b}]_{2N\times 2N}[T^{\mathrm{Exp}}]_{2N\times 2N}[T_{a,l_a}]_{2N\times 2N}. \tag{B2}$$

$[T_{a,l_a}]_{2N\times 2N}$ is the transfer matrix of straight duct with radius a and length l_a. $[T_{b,l_b}]_{2N\times 2N}$ is the transfer matrix of straight duct with radius b and length l_b.

The transfer matrix of an expansion $[T^{\mathrm{Exp}}]_{2N\times 2N}$ is deduced by inversing the transfer matrix of the constriction matrix given by

$$[T^{\mathrm{Const}}]_{2N\times 2N} = \begin{bmatrix} [F]_{N\times N} & [0]_{N\times N} \\ [0]_{N\times N} & [G]^{-1}_{N\times N} \end{bmatrix}_{2N\times 2N}. \tag{B3}$$

$[F]_{N\times N}$ and $[G]_{N\times N}$ are deduced from the continuity boundary conditions on pressure and axial particle velocity in the duct crosssection S where the area modification occurs:[8]

$$F_{pq,mn} = \frac{1}{N^b_{pq}}\int\int_{S_b}\Psi^a_{mn}\Psi^{b*}_{pq}rdrd\theta, \tag{B4}$$

$$G_{mn,pq} = \frac{1}{N^a_{mn}}\int\int_{S_a}\Psi^b_{pq}\Psi^{a*}_{mn}rdrd\theta.$$

$N^{b,a}_{mn} = S_{b,a}J^2_m(\chi_{mn})[1-(m^2/\chi^2_{mn})]$ is the normalization factor. $S_a = \pi(a)^2$ and $S_b = \pi(b)^2$.

APPENDIX C: COMPUTATION OF THE PRESSURE IN THE TWO PAIRS OF DUCT CROSS SECTIONS DURING THE SIMULATION PROCEDURE OF THE EXPERIMENT

The expression of the incident pressure $\{P^{\mathrm{I}+}_{mn}(z_L)\}_N$ distributed on N cut-on modes produced by a point source (Fig. 6) in the semi-infinite duct at z_L is given by[8]

$$\{P^{\mathrm{I}+}_{mn}(z_L)\}_N = \{\alpha_{mn}A_S e^{i(\varphi_S - m\theta_S + k_{mn}(z_L - z_S))}\}_N, \tag{C1}$$

where $\alpha_{mn} = 1/2ik_{mn}N^a_{mn}$, $A_S = 1$, and $\varphi_S = 0$ are, respectively, the phase and amplitude of the point source, θ_S and z_S are angular and axial positions of the point source.

The transmission matrix $[T_R]_{N\times N}$ of the duct element (Fig. 6) located between z_L and z_R is defined as a function of the incident and transmitted pressures distributed on the cut-on modes of the main duct by[9]

$$\{P^{\mathrm{II}+}_{mn}(z_R)\}_N = [T_R]_{N\times N}\cdot\{P^{\mathrm{I}+}_{mn}(z_L)\}_N. \tag{C2}$$

If $[R^I(z_L)]_{N\times N}$ and $[R^{\mathrm{II}}(z_R)]_{N\times N}$ are the reflection matrices in both cross-section areas located at z_L and z_R apart from the discontinuity (Fig. 7) the incident and reflected pressures in z_L and z_R distributed on cut-on modes of the main duct are related by

$$\{P^{\mathrm{II}-}_{mn}(z_R)\}_N = [R^{\mathrm{II}}(z_R)]_{N\times N}\cdot\{P^{\mathrm{II}+}_{mn}(z_R)\}_N \quad \text{and} \tag{C3}$$

$$\{P^{\mathrm{I}-}_{mn}(z_L)\}_N = [R^{\mathrm{I}}(z_L)]_{N\times N}\cdot\{P^{\mathrm{I}+}_{mn}(z_L)\}_N.$$

The reflection matrix in z_R is deduced from the reflection matrix $[R^{\mathrm{II}}(z_{\mathrm{end}})]_{N\times N}$ in the open cross-section area located at z_{end} computed from a theoretical model which assumes an infinite baffle condition.[21]

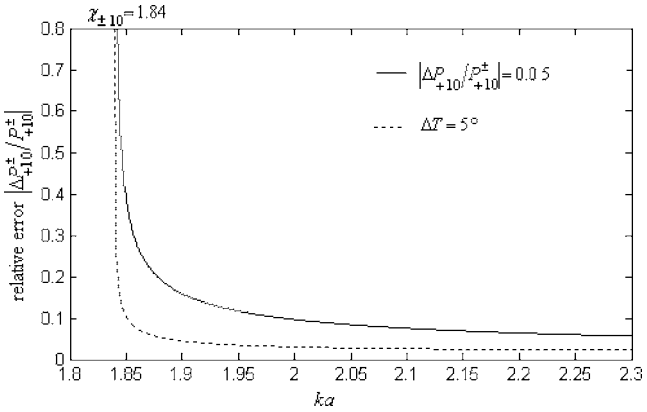

FIG. 22. The relative uncertainty vs *ka* on the determination of the incident (1,0) modal pressure by the separation technique to 5° in *T* or 5% in modulus of total modal coefficient.

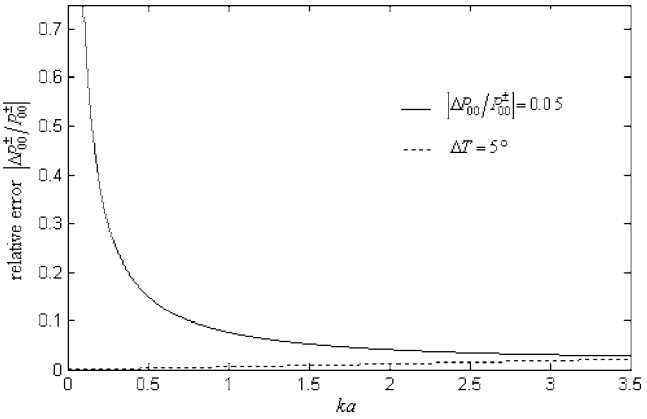

FIG. 23. The relative uncertainty vs *ka* on the determination of the incident plane wave pressure by the separation technique to 5° in *T* or 5% in modulus of total modal coefficient.

$$[R^{\mathrm{II}}(z_R)]_{N\times N} = [\mathrm{diag}(e^{-ik_{mn}E})]^{-1}_{N\times N} \cdot [R^{\mathrm{II}}(z_{\mathrm{end}})]_{N\times N} \times [\mathrm{diag}(e^{+ik_{mn}E})]_{N\times N}. \quad \text{(C4)}$$

$[T_R]_{N\times N}$ and $[R^{\mathrm{I}}(z_L)]_{N\times N}$ are deduced from the scattering matrix for a given length *E* load with the relationships:

$$[T_R]_{N\times N} = [[I]_{N\times N} - [S^{22}]_{N\times N} \cdot [R^{\mathrm{II}}(z_R)]_{N\times N}]^{-1}_{N\times N} \cdot [S^{21}]_{N\times N}, \quad \text{(C5)}$$

$$[R^{\mathrm{I}}(z_L)]_{N\times N} = [[S^{11}]_{N\times N} + [S^{12}]_{N\times N} \cdot [R^{\mathrm{II}}(z_R)]_{N\times N} \cdot [T_R]_{N\times N}]_{N\times N}. \quad \text{(C6)}$$

The total acoustic pressures in the four cross sections located at z_L, z_{L+d}, z_R, and z_{R+d} are then deduced by adding the incident and reflected pressures:

$$\{P^{\mathrm{I,II}}_{mn}(z_{L,R})\}_N = \{P^{\mathrm{I,II+}}_{mn}(z_{L,R})\}_N + \{P^{\mathrm{I,II-}}_{mn}(z_{L,R})\}_N, \quad \text{(C7)}$$

$$\{P^{\mathrm{I,II}}_{mn}(z_{L,R}+d)\}_N = [\mathrm{diag}(e^{+ik_{mn}d})]_{N\times N} \cdot \{P^{\mathrm{I,II+}}_{mn}(z_{L,R})\}_N + [\mathrm{diag}(e^{-ik_{mn}d})]_{N\times N} \cdot \{P^{\mathrm{I,II-}}_{mn}(z_{L,R})\}_N. \quad \text{(C8)}$$

This calculation is performed for $q=1$, *N* source configurations $(z_S, \theta_S)^q$ and all loads (Table I).

APPENDIX D: ANALYTIC SOLUTION OF THE ERROR CALCULATION ISSUED FROM THE SEPARATION TECHNIQUE

The complex incident and reflected modal pressures P^{+}_{mn} and P^{-}_{mn} are solutions of the following system[19] where $P^{1,2}_{mn}$ are the total modal pressures in two cross sections separated by a distance *d* (Fig. 2):

$$P^{+}_{mn} = \frac{P^{1}_{mn}e^{-ik_{mn}d} - P^{2}_{mn}}{e^{-ik_{mn}d} - e^{ik_{mn}d}},$$

$$P^{-}_{mn} = \frac{P^{2}_{mn} - P^{1}_{mn}e^{ik_{mn}d}}{e^{-ik_{mn}d} - e^{ik_{mn}d}}. \quad \text{(D1)}$$

If $\Delta P^{1,2}_{mn}$, Δk_{mn}, and Δd are, respectively, the uncertainties on the total modal pressures $P^{1,2}_{mn}$, axial wave number, and distance, the error on $P^{\pm}_{mn}$ can be deduced from

$$\Delta P^{\pm}_{mn} \simeq \xi^{\pm}_{mn}\Delta P_{mn} + \eta^{\pm}_{mn}(d\Delta k_{mn} + k_{mn}\Delta d), \quad \text{(D2)}$$

where

$$\xi^{\pm}_{mn} = \frac{\partial P^{\pm}_{mn}}{\partial P^{1}_{mn}} + \frac{\partial P^{\pm}_{mn}}{\partial P^{2}_{mn}} = \frac{\pm e^{\mp ik_{mn}d} \pm 1}{e^{-ik_{mn}d} - e^{ik_{mn}d}},$$

$$\eta^{\pm}_{mn} = \frac{\partial P^{\pm}_{mn}}{\partial (k_{mn}d)} = \pm 2 \cdot i\left(\frac{P^{1}_{mn} - P^{2}_{mn}\cos(k_{mn}d)}{(e^{-ik_{mn}d} - e^{ik_{mn}d})^2}\right).$$

Assuming a reflecting condition where the conversion is neglected:

$$P^{-}_{mn} = P^{+}_{mn}R_{mn,mn} \Rightarrow \begin{cases} P^{1}_{mn} = P^{+}_{mn}(1 + R_{mn,mn}) \\ P^{2}_{mn} = P^{+}_{mn}(e^{ik_{mn}d} + e^{-ik_{mn}d}R_{mn,mn}) \end{cases}$$

the coefficient $\eta^{\pm}_{mn}$ becomes

$$\eta^{\pm}_{mn} = \pm 2iP^{+}_{mn}\left(\frac{(1 - e^{ik_{mn}d}\cos(k_{mn}d)) + R_{mn,mn}(1 - e^{-ik_{mn}d}\cos(k_{mn}d))}{(e^{-ik_{mn}d} - e^{ik_{mn}d})^2}\right).$$

If the hard wall reflection condition $|R_{mn,mn}|=1$ and $\Phi(R_{mn,mn})=0$ is assumed, $\eta^{\pm}_{mn}=\pm iP^{+}_{mn}$ and Eq. (D2) is lead-ing to the relationship which gives the error on the incident and reflected modal pressure relative to the incident modal pressure:

$$\Delta P^{\pm}_{mn}/P^{\pm}_{mn} \simeq \xi^{\pm}_{mn} \cdot (\Delta P_{mn}/P^{\pm}_{mn}) + i(d \cdot \Delta k_{mn} + k_{mn} \cdot \Delta d). \tag{D3}$$

The uncertainty Δk_{mn} on the axial wave number k_{mn} is deduced from the uncertainties on T the temperature and on f^c_{mn} cut-off frequency of mode (m,n) by

$$\Delta k_{mn} \simeq \frac{\partial k_{mn}}{\partial c_0}\frac{\partial c_0}{\partial T}\Delta T + \frac{\partial k_{mn}}{\partial f^c_{mn}}\Delta f^c_{mn} = \mu'_{mn}\Delta T + \mu_{mn}\Delta f^c_{mn}, \tag{D4}$$

where $c_0 = 20\sqrt{273+T} \simeq 330.45 + 0.607T$. As

$f^c_{mn} = \frac{c_0}{2\pi}\frac{\chi_{mn}}{a}$, it is easy to show that

$$\Delta f^c_{mn} \simeq 0.607\frac{\chi_{mn}}{2\pi a}\Delta T + \frac{c_0}{2\pi a}\Delta\chi_{mn} + \frac{\chi_{mn}c_0}{2\pi a^2}\Delta a, \tag{D5}$$

where $\mu_{mn} = (2\pi/c_0)^2 f^c_{mn}/k_{mn}$ and $\mu'_{mn} \simeq 0.607 k_{mn}/c_0$. $\Delta\chi_{mn}$ is an error issued from the measurement duct wall boundary condition and Δa the error on the measurement duct radius.

From the relationships (D3) and (D4) the relative uncertainty $\Delta P^+_{mn}/P^+_{mn}$ to errors in T, χ_{mn}, a can then be deduced. The contributions to the relative error $\Delta P^+_{mn}/P^+_{mn}$ vs ka of a 5° error in temperature and 5% error in the modulus of the total modal pressure are plotted in Fig. 22 for a mode $(1,0)$ and Fig. 23 for the plane wave. These curves point out that for the plane case the error on the pressure measurement is more important than this on the temperature as shown in a previous study[20] while for a higher order mode both contributions are similar in amplitude and become very sensitive when the frequency tends to be near to the cut-off mode frequency.

[1] M. L. Munjal, *Acoustics of Ducts and Mufflers* (Wiley-Interscience, New York, 1987).
[2] P. O. A. L. Davies, "Practical flow duct acoustics," J. Sound Vib. **124**, 91–115 (1988).
[3] R. Glav and M. Aböm, "A general formalism for analyzing acoustic 2-port network," J. Sound Vib. **202**(5), 739–747 (1997).
[4] W. Evermans, "A systematic procedure for the analysis of multiply branched acoustic transmission lines," Trans. ASME, J. Vib., Acoust., Stress, Reliab. Des. **109**, 168–177 (1987).
[5] Y. Auregan and R. Starobinski, "Determination of acoustical energy dissipation/production potentiality from the acoustical transfer functions of a multiport," Acust. Acta Acust. 85, 788–792 (1999).
[6] Z. Tao and A. F. Seybert, "A review of current techniques for measuring mufflers transmission loss," Soc. Auto. Eng. 03NVC-38, 2001.
[7] M. Abom, "Measurement of the scattering matrix of acoustical two-ports," Mech. Syst. Signal Process. **5**(2), 89–104 (1991).
[8] M. Akoum and J. M. Ville, "Measurement of reflection matrix of a discontinuity in a duct," J. Acoust. Soc. Am. **103**(5), 2463–2468 (1998).
[9] A. Sitel, J. M. Ville, and F. Foucart, "An experimental facility for measurement of acoustic transmission matrix and acoustic power dissipation of duct discontinuity in higher order modes propagation conditions," Acust. Acta Acust. 89, 586–594 (2003).
[10] R. T. Muehleisen and D. C. Swanson, "Modal coupling in acoustic waveguides: Planar discontinuities," Appl. Acoust. **63**, 1375–1392 (2002).
[11] P. M. Morse and K. U. Ingard, *Theoretical Acoustics* (McGraw-Hill, New York, 1968).
[12] E. R. Rademaker *et al.*, Publishable Synthesis Report No. DUCAT-NL-01, 2001.
[13] J. M. Auger and J. M. Ville, "Measurement of liner impedance based on the determination of duct eigenvalues by Fourier-Lommel's transform," J. Acoust. Soc. Am. **88**, 19–22 (1990).
[14] H. Boden and M. Abom, "Influence of errors on the two-microphone method for measuring acoustic properties in ducts," J. Acoust. Soc. Am. **79**(2), 541–549 (1985).
[15] J. Lavrenjev and M. Äbom, "Characterisation of fluid machines as acoustic multi-port sources," J. Sound Vib. **197**(1), 1–16 (1996).
[16] H. Bodèn, "The multiple load method for measurement of the source characteristics of time-variant sources," J. Sound Vib. **148**(3), 437-453 (1991).
[17] G. H. Golub and C. F. Loan, *Matrix Computations* (North Oxford Academic, Oxford, 1983).
[18] J. M. Auger and J. M. Ville, "Flow effects on measurement of the modal decomposition of acoustic field in a hard cylindrical duct," Proceedings of the Aero and Hydro Acoustics IUTAM Symposium, Lyon, France, 1985, pp. 437–443.
[19] M. Abom, "Modal decomposition in ducts based on transfer function measurements between microphone pairs," J. Sound Vib. **135**(1), 95–114 (1989).
[20] R. T. Muehleisen and C. W. Beamer IV, "Comparison of errors in the three and four microphone method used in the measurement of acoustic properties of porous materials," ARLO **3**(4), 112–117 (2002).
[21] W. E. Zorumski, "Generalized radiation impedance and reflection coefficients of circular and annular ducts," J. Acoust. Soc. Am. **54**, 1667–1673 (1973).